

Electromigration in thin tunnel junctions with ferromagnetic/nonmagnetic electrodes: Nanoconstrictions, local heating, and direct and wind forces

J. Ventura* and J. B. Sousa†

IFIMUP and Faculty of Sciences U. Porto, Rua do Campo Alegre, 678, 4169-007, Porto, Portugal

Y. Liu, Z. Zhang, and P. P. Freitas‡

INESC-MN and IST, Rua Alves Redol, 9-1, 1000-029 Lisbon, Portugal

(Received 3 May 2005; revised manuscript received 12 July 2005; published 27 September 2005)

Current Induced Resistance Switching (CIS) was recently observed in thin tunnel junctions with ferromagnetic (FM) electrodes, i.e., FM/I/FM. This effect was attributed to electromigration of metallic atoms in nanoconstrictions in the insulating barrier (I). Here we study how the CIS effect is influenced by a thin nonmagnetic (NM) Ta layer, deposited just below the AlO_x insulating barrier in tunnel junctions of the type FM/NM/I/FM (FM=CoFe). Enhanced resistance switching occurs with increasing maximum applied current (I_{max}), until a plateau of constant CIS is reached for $I_{\text{max}} \sim 65$ mA (CIS $\sim 60\%$) and above. However, such high electrical currents also lead to a large ($\sim 9\%$) irreversible resistance decrease, indicating barrier degradation. Anomalous voltage-current characteristics with negative derivative were also observed near $\pm I_{\text{max}}$ and this effect is here attributed to heating in the tunnel junction. One observes that the current direction for which resistance switches in FM/NM/I/FM (clockwise) is opposite to that of FM/I/FM tunnel junctions (anticlockwise). This effect will be discussed in terms of a competition between the electromigration contributions due to the so-called direct and wind forces. It will be shown that the direct force is likely to dominate electromigration in the Ta (NM) layers, while the wind contribution likely dominates in the CoFe (FM) layers.

DOI: [10.1103/PhysRevB.72.094432](https://doi.org/10.1103/PhysRevB.72.094432)

PACS number(s): 66.30.Pa, 66.30.Qa, 73.40.Gk, 73.40.Rw

I. INTRODUCTION

Tunnel junctions (TJ) consisting of two ferromagnetic (FM) layers separated by an insulator (I)¹ show enormous potential for a multiplicity of applications such as read head,² strain,³ current, position and speed⁴ sensors or even to detect magnetically tagged biological specimens.⁵ However, probably the most sought after application is high performance, low cost, nonvolatile magnetoresistive random access memories (MRAMs).⁶ In a tunnel junction, the magnetization of one of the FM layers (pinned layer) is fixed by an underlying antiferromagnetic (AFM) layer. The magnetization of the other FM layer (free layer) reverses almost freely when a small magnetic field is applied. Due to spin dependent tunneling⁷ one obtains two distinct resistance (R) states corresponding to pinned and free layer magnetizations parallel (low R) or antiparallel (high R). However, several drawbacks are still of concern in actual MRAM submicron devices, like cross-talk in the array configuration or the large power consumption to generate the magnetic field to switch R. One then aims to replace the magnetic field-driven magnetization reversal by a Current Induced Magnetization Switching (CIMS) mechanism.^{8,9} Such goals were recently achieved in magnetic tunnel junctions^{10,11} for current densities $j \sim 10^7$ A/cm². On the other hand, Liu *et al.*¹² observed reversible resistance changes induced by lower current densities ($j \sim 10^6$ A/cm²) in thin FM/I/FM TJs. These changes, although initially attributed to the CIMS mechanism, were later found¹³ not dependent on the relative orientation of the magnetizations of the free and pinned layers. This effect was then called Current Induced Switching (CIS) and is now attributed^{14,15} to electromigration (EM) in nanoconstrictions

in the insulating barrier. The combination of the tunnel magnetoresistive and CIS effects allows the use of a magnetic tunnel junction as a three resistance state device.¹⁶ Both CIS and CIMS effects seem to coexist in thin magnetic tunnel junctions for $j \gtrsim 10^6$ A/cm². The reasons for the observed dominance of one effect over the other are still unclear but likely related to structural differences in the tunnel junctions. One notes, however, that electromigration can in fact limit the implementation of the spin torque mechanism in actual devices and be a major reliability issue in read head sensors.¹⁷

When a metal is subjected to an electrical field \mathbf{E} , the usual random diffusive motion of atoms is biased by the resulting driving force \mathbf{F} , and a net atomic flux can be observed. This phenomena is known as electromigration¹⁸ and \mathbf{F} can be written as:

$$\mathbf{F} = Z^* e \mathbf{E}, \quad (1)$$

where Z^* is the effective valence and e is the elementary charge. The force acting on the migrating ion is usually separated into two components, both linear in the external applied electrical field:

$$\mathbf{F} = \mathbf{F}_d + \mathbf{F}_w = (Z_d + Z_w) e \mathbf{E}. \quad (2)$$

The direct force \mathbf{F}_d arises from the electrostatic interactions between the electrical field and the so-called direct valence of the ion Z_d (>0). The theoretical calculation of the direct force is a challenging process but $Z_d \approx Z$ (Z =ion valence) is usually assumed. The wind force \mathbf{F}_w results from momentum exchange between the current carrying electrons and the migrating ions and so it has the direction of the electron current

(opposite to the electrical field). The wind valence Z_w is simply a convenient term to describe the wind force, arising from the fact that \mathbf{F}_w is proportional to the current density and, in an ohmic material, to \mathbf{E} . The competition between wind and direct forces is often dominated by the first, which usually controls the sign and magnitude of the effective valence Z^* and the EM process.

Here we study how a Ta nonmagnetic (NM) amorphous thin layer deposited just below the insulating barrier influences the Current Induced Switching. In a CIS cycle, the resistance commutes between two states due to electromigration of ions from the electrodes into the barrier (decreasing R) and from the barrier back into the electrodes (increasing R).¹⁴ We can then define the CIS coefficient as the relative difference between these two R-states. Interestingly, the current direction for which R-switching occurs in FM/NM/I/FM tunnel junctions is opposite to that of FM/I/FM tunnel junctions.¹⁵ Using the intuitive ballistic model of EM, we will show that the direct force is likely to dominate electromigration in Ta (NM) layers, while the wind force dominates in CoFe (FM) layers. The switching direction difference will be here associated with the dominance of different EM forces (direct or wind) in the two types of tunnel junctions referred.

The CIS coefficient was strongly enhanced by increasing the maximum applied current (I_{\max}), reaching almost 60% for $I_{\max}=80$ mA. However, severe R-degradation occurs when $I_{\max} \geq 65$ mA. Voltage-current characteristics show strong anomalous nonlinearities, here associated with heating effects. Comparing our experimental results with voltage-current characteristics as predicted by Simmons' model,¹⁹ we estimate that the temperature inside the tunnel junction reaches ~ 600 K for $I_{\max}=80$ mA. Numerical results from a model of heat generation in tunnel junctions suggest that such high temperatures can only occur if local current densities much larger than $j=I/A$ (I the electrical current and A the total tunnel junction area) exist within the barrier. One concludes that these hot-spots concentrate most of the current flowing through the tunnel junction stack and are likely the reason for the occurrence of EM in the studied tunnel junctions.

II. ELECTROMIGRATION

For atomic diffusion to occur, an atom needs to surmount the energy barrier E_b separating neighboring equilibrium lattice sites [Fig. 1(a)]. When an electric current flows through a metal this usual, thermally activated, random motion of atoms is biased by the electrical field [Fig. 1(b)], resulting in a net atomic flow. This phenomena is known as electromigration¹⁸ and is currently the major cause of failure of interconnects in integrated circuits.²⁰ Studies of EM in interconnects are performed under severe conditions, such as high electrical current densities ($\sim 10^7$ A/cm²) and temperature (~ 500 – 700 K) and show that EM can occur through different diffusion paths, such as grain boundary and interfaces, as in Al²¹ and Cu²² interconnects, respectively. The relative importance of the different diffusion paths varies with the material properties, such as grain size and orientation, interface bonding and structure.

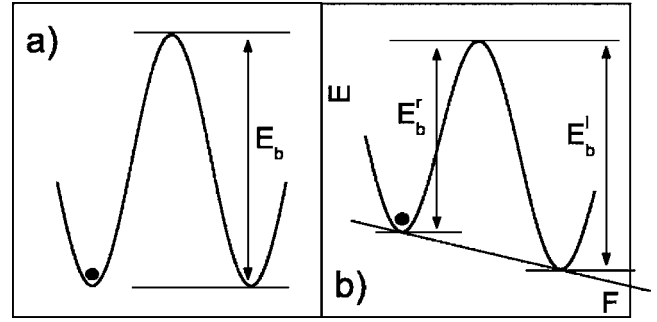


FIG. 1. Energy barrier for atomic diffusion, (a) without and (b) with an applied electrical field. Notice how the direction for diffusion becomes biased by the driving force F : The energy barrier for migration to the right (E_b^r) is smaller than that for migration to the left (E_b^l).

Electromigration is also a concern in magnetic nanostructures, namely spin valves and tunnel junctions.¹⁷ During device operation, local structural inhomogeneities can lead to large current density, and thus to electromigration. This is of particular importance in tunnel junctions where the resistance depends exponentially on the barrier thickness and where localized nanoconstrictions can concentrate most of the current. Such high current densities can also produce intense heating leading to enhanced electromigration.¹⁷ Discrete electromigration events were observed in metallic nanobridges (for $j \sim 10^8$ A/cm²).²³ Reversible EM was recently observed in Ni nanoconstrictions ($j \sim 10^{13}$ A/cm²)²⁴ and thin tunnel junctions ($j \sim 10^6$ A/cm²).^{12,14} Electromigration in these nanostructures can lead to both an increase and a decrease of the electrical resistance, depending on the sense of the applied electrical current, and thus on the sense of EM-driven atomic motion.

The ballistic model of electromigration presents the most intuitive picture of the underlying physics of EM. The wind force is calculated assuming that all the momentum lost by the scattered electrons is transferred to the migrating ion.²³ In the free electron approximation the wind valence becomes:¹⁸

$$Z_w = -n l \sigma_{tr}, \quad (3)$$

where n is the electron density, l is the electron mean free path, and σ_{tr} is the electron transport cross section for scattering by the ion. Using, e.g., known values for Fe ($n \sim 10^{-1}$ Å⁻³, $l \sim 50$ Å, $\sigma_{tr} \sim 3$ Å²),^{25,26} one finds $Z_w \sim -15$ ($|Z_w| \gg Z \approx 2$). Such estimative confirms that the wind force usually dominates electromigration. More elaborated EM models such as the pseudopotential method give lower Z_w values, by as much as 70%.¹⁸ However, because of its simplicity, we will use the ballistic model to qualitatively explain our results.

Sorbello²⁷ first studied electromigration forces in mesoscopic systems. In particular he considered electromigration near a point contact, modeled as a circular aperture of radius a between two metallic layers of electrical resistivity ρ . He found that the direct force is then greatly enhanced near such constriction. An estimate on the relative magnitude of the wind and direct forces gives:^{23,27}

$$\frac{F_w}{F_d} \propto -\frac{a\sigma_{lr}}{Z_d}, \quad (4)$$

which evidences the important role played by the constriction geometry: The smaller the constriction radius, the larger will be the direct force compared to the wind force.

III. EXPERIMENTAL DETAILS

In this work we used a series of ion beam deposited tunnel junctions, with a nonmagnetic Ta layer inserted just below the insulating AlO_x barrier. The complete structure of the tunnel junctions studied was glass/bottom lead/Ta (90 Å)/NiFe (50 Å)/MnIr (90 Å)/CoFe (40 Å)/Ta (20 Å)/ AlO_x (3 Å+4 Å)/CoFe (30 Å)/NiFe (40 Å)/Ta (30 Å)/TiW(N) (150 Å)/top lead. The chosen structure is similar to that of magnetic tunnel junctions grown for actual applications except for the additional Ta layer, thus making a comparison between the FM/I/FM and FM/NM/I/FM systems easier. Previous Transmission Electron Microscopy images obtained in similar samples show no significant microstructural changes induced by a Ta layer deposited below the barrier.²⁸ The AlO_x barrier was formed by two-step deposition and natural oxidation processes (50 mTorr, 3 min, 100 mTorr, 20 min).¹² NiFe, CoFe, MnIr, and TiW(N) stand for $\text{Ni}_{80}\text{Fe}_{20}$, $\text{Co}_{80}\text{Fe}_{20}$, $\text{Mn}_{78}\text{Ir}_{22}$ and $\text{Ti}_{10}\text{W}_{90}(\text{N})$. The bottom and top leads are made of Al 98.5% Si 1% Cu 0.5%, and are 600 Å (26 μm) and 3000 Å (10 μm) thick (wide), respectively. The junctions were patterned to a rectangular shape with area $A=4 \times 1 \mu\text{m}^2$ by a self-aligned microfabrication process.

The electrical resistance, magnetoresistance and current induced switching were measured with a four-point d.c. method, with a current stable to $1:10^6$ and using an automatic control and data acquisition system.

CIS cycles were performed using the pulsed current method¹³ allowing us to measure the *remnant* resistance of the tunnel junction after each current pulse. Current pulses (I_p) of 1 s duration and 5 s repetition period are applied to the junction, starting with increasing negative pulses from $I_p=0$ (where we define the resistance as R_{initial}), in $\Delta I_p=5$ mA steps up to a maximum $+I_{\text{max}}$, dependent on cycle in the 10–80 mA range. One then decreases the current pulses (always with the same ΔI_p), following the reverse trend through zero current pulse (R_{half}) down to negative $-I_{\text{max}}$, and then again to zero (R_{final}), closing the CIS hysteretic cycle, $R=R(I_p)$. Positive current is here defined as flowing from the bottom to the top lead.

The junction remnant resistance is measured in the 5 s-waiting periods between consecutive current pulses, using a low current of 0.1 mA, providing a $R(I_p)$ curve for each cycle. This low current method allows us to systematically discard nonlinear I(V) contributions to the resistance. However, the voltage across the TJ is also measured while applying the current pulse I_p , enabling us to obtain the (nonlinear) $V(I_p)$ characteristic for each CIS cycle.

Using the definitions above, one can define the CIS coefficient as:

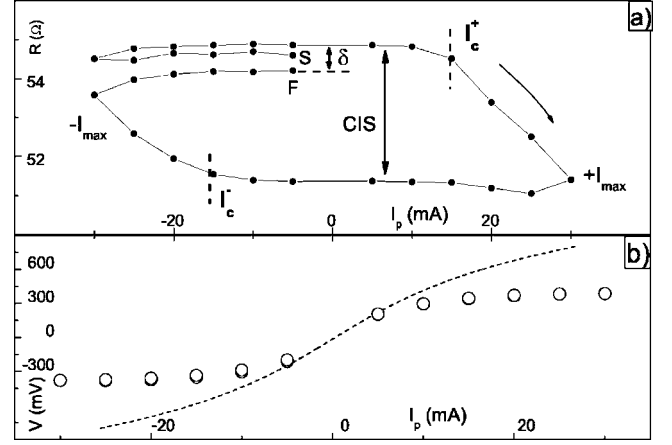


FIG. 2. (a) Current induced switching cycle for $I_{\text{max}}=30$ mA, starting at point S and finishing at F. After each current pulse I_p , the electrical resistance of the tunnel junction is measured under a low bias current, enabling us to obtain the depicted $R(I_p)$ cycle. Effective switching occurs between I_c^+ and $+I_{\text{max}}$, and resistance recovery between I_c^- and $-I_{\text{max}}$. (b) Corresponding experimental (hollow circles) and simulated (dashed line) $V(I_p)$ characteristic. While applying the current pulse I_p , the voltage across the tunnel junction is measured and a $V(I_p)$ characteristic obtained.

$$\text{CIS} = \frac{R_{\text{initial}} - R_{\text{half}}}{(R_{\text{initial}} + R_{\text{half}})/2}. \quad (5)$$

We also define the resistance shift (δ) in each cycle:

$$\delta = \frac{R_{\text{final}} - R_{\text{initial}}}{(R_{\text{initial}} + R_{\text{final}})/2}. \quad (6)$$

IV. EXPERIMENTAL RESULTS

The studied tunnel junction had an initial electrical resistance $R=57.8 \Omega$ and a resistance area product $R \times A = 230 \Omega \mu\text{m}^2$. No magnetoresistance was observed in our tunnel junctions, due to the loss of interfacial polarization (20 Å Ta layer deposited just below the barrier). In fact, the tunnel magnetoresistance of a TJ is known to exponentially decrease with the thickness of a nonmagnetic layer inserted just below the insulating barrier^{28,29} and TMR then goes rapidly to zero within the first monolayers of the nonmagnetic material.

We measured CIS cycles with increasing I_{max} , starting with a cycle up to $I_{\text{max}}=30$ mA [Fig. 2(a); cycle starting at point S] giving CIS=9.2% and $\delta=-3.5\%$. No resistance switching was observed under the initial negative current pulses ($I_p=0 \rightarrow -I_{\text{max}}$). However, upon reversing the current one observes that for $I_p \geq 15$ mA [where we define the positive critical current I_c^+ ; see Fig. 2(a)] the resistance starts to decrease, a trend which becomes increasingly enhanced (switching) with I_p , up to $I_{\text{max}}=30$ mA. This switching is associated with electromigration of metallic ions from the electrodes into the barrier,^{14,15} decreasing the effective barrier thickness and consequently the junction resistance. The previous absence of R-switching under negative current

pulses indicates an electromigration asymmetry with respect to the electrode/oxide interfaces, i.e., only ions from one such interface are actively participating in electromigration. Physically such asymmetry arises not only from the different materials deposited just below (Ta) and above (CoFe) the insulating barrier, but also from the deposition and oxidation processes during tunnel junction fabrication. In particular the top electrode is deposited over an oxidized *smooth* surface, while a much more irregular bottom electrode/oxide interface is experimentally observed.³⁰ Since the migration of ions into and out of the barrier should occur preferentially in nanoconstrictions (higher electrical fields), one concludes that such ions likely belong to the Ta bottom electrode. The current density and electrical field at R-switching can be estimated as $j_c \sim 0.375 \times 10^6 \text{ Acm}^2$ and $E_c \sim 3 \text{ MV/cm}$, respectively.

Returning to Fig. 2(a), the subsequent decrease of I_p from $+I_{\max}$ to zero hardly affects the low resistance state. However, for $I_p \leq -15 \text{ mA}$ (where we define the negative critical current I_c^-), the resistance gradually increases until $I_p = -I_{\max}$, recovering a significant fraction of the previous R-switching near $+I_{\max}$. This indicates that, under a reversed electrical field, many ions return to their initial sites. The subsequent change of I_p from $-I_{\max}$ to zero (to close the CIS cycle at point F) produces no significant change in resistance. However, the final resistance mismatch ($R_{\text{final}} < R_{\text{initial}}$; $\delta = -3.5\%$) indicates some irreversible effects in this CIS cycle ($I_{\max} = 30 \text{ mA}$), associated with barrier degradation.

The voltage across the junction was also measured for each applied current pulse (I_p), providing the $V(I_p)$ characteristic depicted in Fig. 2(b) (hollow circles). If one uses Simmons' model¹⁹ to fit this curve with adequate thin TJ barrier parameters¹⁴ (barrier thickness $t = 9 \text{ \AA}$, barrier height $\phi = 1 \text{ eV}$), the quality of the fit is poor [dashed line in Fig. 2(b)], with large discrepancies near $\pm I_{\max}$. Also, the use of the Brinkman model for asymmetric tunnel junctions³¹ does not yield good fits. Such discrepancies near $\pm I_{\max}$ are related to localized heating inside the tunnel junction, as discussed below.

We then performed CIS cycles with increasing I_{\max} , from 30 to 80 mA, in $\Delta I_{\max} = 5 \text{ mA}$ steps as shown for representative cycles in Fig. 3. Notice the enhanced R-switching and R-recovering stages (vs I_p), occurring from I_c^+ to I_{\max} and from I_c^- to $-I_{\max}$, respectively. From these data one can obtain the CIS and δ -shift in each cycle, obtaining the corresponding dependence on I_{\max} as depicted in Fig. 4. The CIS coefficient rises with I_{\max} until $\sim 65 \text{ mA}$ (CIS = 57.4%), saturating for higher current pulses. On the other hand, δ remains fairly small below $I_{\max} \sim 60 \text{ mA}$ ($\delta = -0.4\%$), but increases rapidly for higher I_{\max} ($\delta = -9.6\%$ for $I_{\max} = 80 \text{ mA}$). The CIS increase with I_{\max} indicates that electromigrated ions are further pushed into the barrier (further lowering R) or/and more ions participate in the EM processes. Ultimately irreversible damage occurs in the barrier, as reflected in the δ -shift enhancement for $I_{\max} > 60 \text{ mA}$ (Fig. 4).

V. DISCUSSION

The observed resistance switching (R decrease) occurs only for *positive* current pulses in the here studied FM/NM/

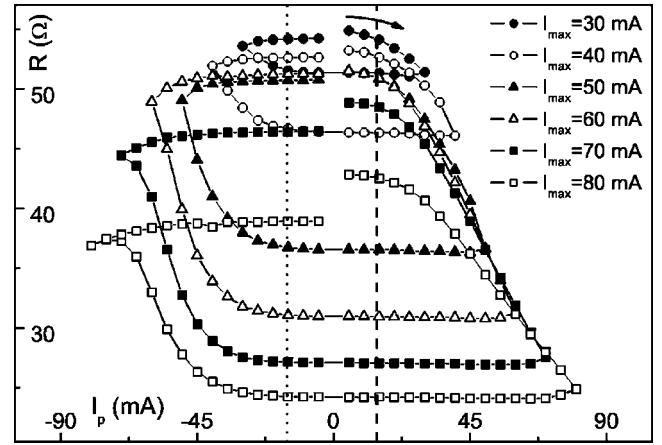


FIG. 3. Selected CIS cycles performed with I_{\max} up to 80 mA. Notice the enhanced R-switching occurring under increasing I_{\max} .

I/FM tunnel junctions [R-recovery occurs under negative I_p ; see Figs. 2(a), 3, and 5], whereas in the previously studied FM/I/FM¹⁵ tunnel junctions switching (recovery) occurs under *negative* (positive) currents [Fig. 5(b); $A = 2 \times 1 \mu\text{m}^2$]. To explain such different behavior one will compare electromigration direct and wind forces in Ta (NM) and CoFe (FM) layers. Using Eq. (3) we obtain:

$$\frac{Z_w(\text{Ta})}{Z_w(\text{CoFe})} = \frac{\rho(\text{CoFe})v_F(\text{Ta})\sigma_{tr}(\text{Ta})}{\rho(\text{Ta})v_F(\text{CoFe})\sigma_{tr}(\text{CoFe})} \quad (7)$$

where v_F is the Fermi velocity. Inserting the parameters given in Table I^{25,26,32,33} one obtains $Z_w(\text{Ta}) \sim 0.07Z_w(\text{CoFe})$. The wind force is then much larger in CoFe than in Ta layers and likely dominates electromigration in the CoFe layers. On the contrary, because Ta is in an amorphous state (notice its high electrical resistivity in Table I), one expects the small electron mean free path to prevent large momentum gains by electrons between consecutive collisions. Using the value estimated previously for $Z_w(\text{Fe})$, one finds $Z_w(\text{Ta}) \sim -1.4[\approx Z_d(\text{Ta})]$. Remembering that the mag-

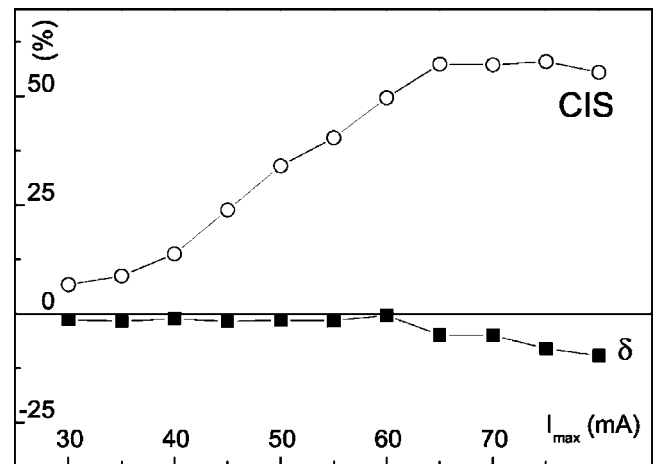


FIG. 4. Current Induced Switching coefficient and δ -shift as a function of maximum applied current. Large δ -shift values occur for $I_{\max} > 60 \text{ mA}$, indicating progressive barrier degradation.

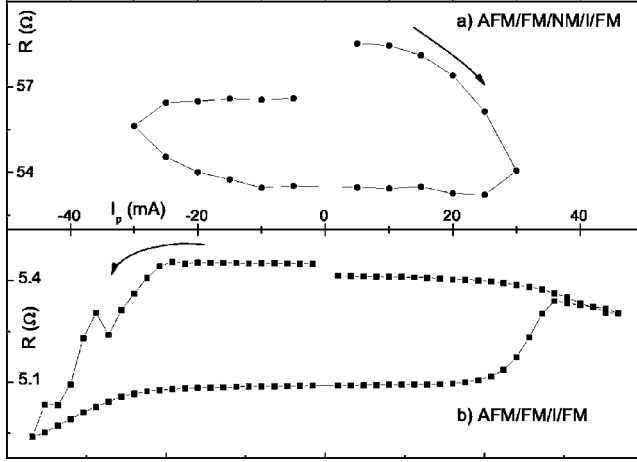


FIG. 5. Resistance switching directions for (a) AFM/FM/NM/I/FM (MnIr/CoFe/Ta/AlO_x/CoFe/NiFe) and (b) AFM/FM/I/FM (MnIr/CoFe/AlO_x/CoFe/NiFe) (Ref. 15) tunnel junctions.

nitude of the direct force is enhanced relatively to the wind force in nanoconstrictions [Eq. (4); see also below] and that the ballistic model overestimates Z_w , one expects the direct force to dominate in Ta. Thus, the likely cause for the observed difference in the R-switching directions is related to the dominance of different electromigration forces in Ta and CoFe. Confirming this conclusion, tunnel junctions with Ta layers deposited just below and just above the insulating barrier (FM/NM/I/NM/FM; not shown) display the same current switching direction as those with only one Ta layer below the insulating barrier (FM/NM/I/FM). On the other hand, when a single NM Ta layer is deposited just above the barrier (FM/I/NM/FM), the R-switching direction is that of FM/I/FM tunnel junctions.

Figure 6 (left scale) shows the CIS $R(I_p)$ -cycle obtained at room temperature, with $I_{\max}=80$ mA (CIS=55.5%; $\delta=-9.6\%$). Notice the $R(I_p)$ -switching from $I_c^+=15$ mA to $I_{\max}=80$ mA and resistance recovery from $I_c^-=-35$ mA to $-I_{\max}=-80$ mA. The $V(I_p)$ characteristic is also displayed (hollow circles; right scale), showing an anomalous plateau with a slight dV/dI_p negative slope for $|I_p| \geq 30$ mA. This effect cannot be explained by tunnel transport theories and is here related to heating inside the tunnel junction. Using our temperature dependent R-data,³⁴ the temperature inside the tunnel junction is estimated as ~ 600 K. Such high temperatures have also been observed in similar measurements performed in FM/I/FM tunnel junctions.¹⁵

Heat generation in tunnel junctions arises from two processes:³⁵ Usual Joule heating in the metallic layers and inelastic electron scattering upon ballistic tunneling. The steady-state heat equation can then be written as:³⁵

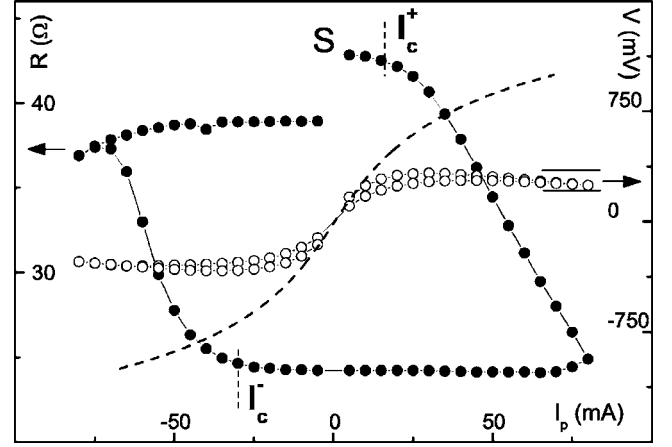


FIG. 6. CIS cycle and corresponding $V(I_p)$ characteristic for $I_{\max}=80$ mA. Notice the decrease of $|V|$ near $\pm I_{\max}$. The dashed line depicts a $V(I)$ curve calculated using Simmons' model.

$$-K \frac{\partial^2 T}{\partial x^2} = \rho j^2 + \frac{jV}{l_{in}} e^{-x/l_{in}} \quad (8)$$

where K is the heat conductivity, T is the temperature, x is the stack position, $j=V/(RA)$ is the current density, V is the bias voltage, and l_{in} is the inelastic scattering electron mean free path. We obtained numerical results assuming that the current density is constant throughout the junction stack. The temperature at the bottom and top of the tunnel junction stack is assumed fixed at 300 K.

Our numerical results (Fig. 7) indicate that large heating can occur near the insulating barrier for high current densities. However, the temperature increase expected from the uniform case, $j_c=I_c/A \sim 0.375 \times 10^6$ A/cm² is negligible (~ 1 K; inset of Fig. 7), and to reach 600 K one needs $j_{est} \sim 16 \times 10^6$ A/cm². This corresponds to an effective area through which current flows $A_{eff}=I_c/j_{est} \approx 0.1$ μm^2 , i.e., about 2.5% of the total tunnel junction area. These results then suggest that j_c is only an *average* value and that nanoconstrictions where the insulating barrier is thinner concentrate most of the current flowing through the junction. Such hot-spots have been observed in similar TJs by atomic force microscopy.³⁵

One can now understand the observed electromigration driven resistance changes in thin FM/NM/I/FM tunnel junctions with NM=Ta [amorphous; Fig. 5(a)]. Under increasing positive current pulses (directed from the bottom to the top lead), the dominating EM direct force induced by the electrical field pushes Ta atoms into the barrier, a process thermally assisted by heating generated by the high current densities flowing in nanoconstrictions. This rises the probability

TABLE I. Electrical resistivity, electron transport cross section for scattering and Fermi velocity used to estimate $Z_w(\text{Ta})/Z_w(\text{CoFe})$.

	$\rho(\mu\Omega \text{ cm})$ (Ref. 33)	$\sigma_\nu(\text{\AA}^2)$ (Ref. 26)	v_F (cm/s) (Refs. 25 and 32)
CoFe	17.1	~ 3	~ 2
Ta	154.0	~ 6	0.67

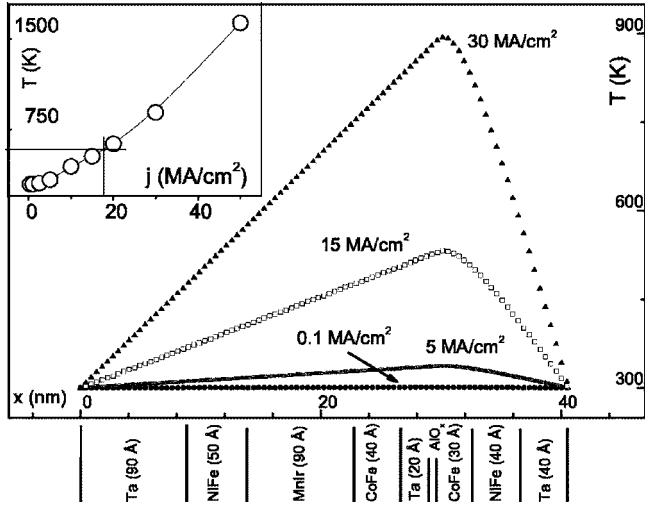


FIG. 7. Simulation of heating processes inside the studied tunnel junction, under different electrical current densities (MA/cm^2). Inset: Temperature increase as a function of current density passing through the junction. The lines show the current density needed for the temperature inside the junction to reach 600 K ($1 \text{ MA} = 10^6 \text{ A}$).

that an atom surmounts the energy barrier for migration E_b (see Fig. 1), greatly enhancing atomic mobility. One notices that even a small barrier weakening (due to such migration) would considerably lower the tunnel resistance due to its exponential dependence on barrier thickness.¹⁹ Using the Simmons' model we can calculate the resistance variation due to a small barrier thickness reduction from t to $t - \delta t$ ($\delta t \ll t$):

$$\frac{R(t) - R(t - \delta t)}{R(t)} = \frac{R_{\text{initial}} - R_{\text{half}}}{R_{\text{initial}}} \approx 1 - e^{-B(\phi)\delta t} \approx B(\phi)\delta t \quad (9)$$

where $B(\phi) = 0.72\sqrt{\phi/2}$. For a CIS coefficient of $\sim 60\%$ one obtains a barrier thickness decrease $\delta t \sim 0.8 \text{ \AA}$. We can now plot the magnitude of the expected δt decrease as a function of the maximum applied current I_{max} (Fig. 8; using the experimental R_{initial} and R_{half} values), which follows the same trend as the CIS coefficient (Fig. 3). In particular, a nonlinear behavior (apparently exponential, as more clearly visible at low temperatures)³⁴ is observed for $I_{\text{max}} \leq 60 \text{ mA}$, that is, while the δ -shift is small and electromigration is mainly reversible. In atomic diffusion processes one often has³⁶ $\partial x / \partial t' \propto F$ (x the position and t' the time). Therefore, in electromigration $\delta t \propto E \delta t'$, i.e., the barrier thickness decrease is proportional to the applied electrical field density and to the migration time $\delta t'$. Following this simple analysis, one has $[R(t) - R(t - \delta t)] / R(t) \propto E$. The CIS effect then depends on how local electrical fields behave near nanoconstrictions and on its dependence on nanostructural atomic rearrangements.

Time dependent measurements (over 4 h) revealed that R remains practically constant both in its high and low state (not shown). This indicates that under a reduced driving force, displaced Ta ions remain trapped in deep enough local energy minima inside lattice potential barriers ($E_b \gg k_B T$), so

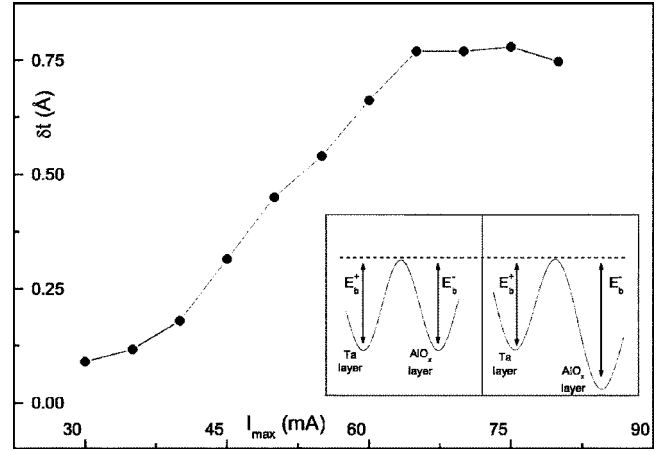


FIG. 8. Dependence of the effective barrier thickness decrease (δt) on the maximum applied current pulse, as obtained from the CIS(I_{max}) curve (Fig. 4) and Eq. (9) (for $\phi = 1 \text{ eV}$). Inset: Energy barrier for migration from Ta into the barrier (E_b^+) and vice versa (E_b^-), in the first (left) and last (right) CIS cycles.

that thermal fluctuations cannot return them to the electrodes. For example, in the CIS cycle of Fig. 5(a) one observes that the low resistance state persists for I_p current pulses from $\approx +I_{\text{max}}$ down to $\approx I_c^-$. However, when $I_p < I_c^-$ the driving force gets strong enough to return displaced ions back into their initial positions in the NM layer. However, the final resistance does not exactly reaches its initial value, indicating progressive barrier degradation. Such degradation should result from metallic ions that remain in the barrier after the CIS cycle is completed. We also notice that in the initial CIS cycle with $I_{\text{max}} = 30 \text{ mA}$ [Fig. 5(a)] one has $I_c^+ \approx |I_c^-|$. This indicates that the driving force for electromigration into and out of the insulating barrier is approximately equal, i.e., the lattice sites where ions migrate to are energetically similar. Furthermore, Fig. 3 (see dashed line) shows that $I_c^+ \approx 15 \text{ mA}$ throughout all the CIS cycles performed, indicating that cycling does not alter the EM force inducing atomic migration from Ta into the barrier. In other words, the energy barrier which the Ta ions surmount when migrating into the barrier is kept constant (inset of Fig. 8). This contrasts with electromigration in the opposite direction, where $|I_c^-|$ increases with cycling (Fig. 3; see dotted line). The force needed to return ions back has to be increased (inset of Fig. 8), indicating that Ta ions migrating under increasingly higher current pulses are pushed further inside the barrier, and are thus more difficult to return to the electrode.

VI. CONCLUSIONS

We studied the Current Induced Switching effect on low resistance (7 \AA barrier) CoFe/Ta/ AlO_x /CoFe tunnel junctions. The CIS coefficient increased with increasing maximum applied current pulses, reaching $\sim 60\%$ for $I_{\text{max}} = 80 \text{ mA}$. Such effect is controlled by nanostructural rearrangements at the electrodes/barrier interfaces, due to ion electro-migration (reversible and irreversible). When high currents are applied, one observes large irreversible resis-

tance decreases. The $V(I_p)$ characteristics showed an anomalous behavior when $|I_{\max}| \geq 65$ mA due to heating effects inside the tunnel junction, showing that the CIS effect is thermally assisted. The analysis of these effects shows that nanoconstrictions indeed concentrate most of the tunneling current through the barrier, forming local hot-spots. One further demonstrates that the R-switching direction is related to a competition between the electromigration contributions due to direct and wind forces: The direct force dominates electromigration in Ta layers, whereas the wind contribution is dominant in CoFe.

Finally, please notice that, although the results presented here concern a single FM/NM/I/FM tunnel junction, they are reproduced when measuring other TJs from the same depo-

sition batch. Particularly, the dependence of the CIS coefficient on maximum applied electrical current is quite similar in different tunnel junctions. The current switching direction is always the same for the same TJ-structure.

ACKNOWLEDGMENTS

Work supported in part by FEDER-POCTI/0155, POCTI/CTM/36489/2000, POCTI/CTM/45252/02, and POCTI/CTM/59318/2004 from FCT and IST-2001-37334 NEXT MRAM projects. J. Ventura is thankful for a FCT doctoral Grant No. SFRH/BD/7028/2001. Z. Zhang and Y. Liu are thankful for FCT post-doctoral Grant Nos. SFRH/BPD/1520/2000 and SFRH/BPD/9942/2002.

*Electronic address: joventur@fc.up.pt

[†]Electronic address: jbsousa@fc.up.pt

[‡]Electronic address: pfreitas@inesc-mn.pt

- ¹J. S. Moodera, L. R. Kinder, T. M. Wong, and R. Meservey, *Phys. Rev. Lett.* **74**, 3273 (1995).
- ²D. Song, J. Nowak, R. Larson, P. Kolbo, and R. Chellew, *IEEE Trans. Magn.* **36**, 2545 (2000).
- ³M. Lohndorf, T. Duenas, M. Tewes, E. Quandt, M. Ruhrig, and J. Wecker, *Appl. Phys. Lett.* **81**, 313 (2002).
- ⁴P. P. Freitas, F. Silva, N. J. Oliveira, L. V. Melo, L. Costa, and N. Almeida, *Sens. Actuators, A* **81**, 2 (2000).
- ⁵H. A. Ferreira, D. L. Graham, P. P. Freitas, and J. M. S. Cabral, *J. Appl. Phys.* **93**, 7281 (2003).
- ⁶S. Tehrani, B. Engel, J. M. Slaughter, E. Chen, M. DeHerrera, M. Durlam, P. Naji, R. Whig, J. Janesky, and J. Calder, *IEEE Trans. Magn.* **36**, 2752 (2000).
- ⁷R. Meservey and P. M. Tedrow, *Phys. Rep.* **238**, 173 (1994).
- ⁸J. C. Slonczewski, *J. Magn. Magn. Mater.* **159**, L1 (1996).
- ⁹L. Berger, *Phys. Rev. B* **54**, 9353 (1996).
- ¹⁰Y. Huai, F. Albert, P. Nguyen, M. Pakala, and T. Valet, *Appl. Phys. Lett.* **84**, 3118 (2004).
- ¹¹G. D. Fuchs, N. C. Emley, I. Krivoritov, P. Braganca, E. M. Ryan, S. Kiselev, J. Sankey, D. C. Ralph, R. A. Buhrman, and J. A. Katine, *Appl. Phys. Lett.* **85**, 1205 (2004).
- ¹²Y. Liu, Z. Zhang, P. P. Freitas, and J. L. Martins, *Appl. Phys. Lett.* **82**, 2871 (2003).
- ¹³Y. Liu, Z. Zhang, and P. P. Freitas, *IEEE Trans. Magn.* **39**, 2833 (2003).
- ¹⁴A. Deac, O. Redon, R. C. Sousa, B. Dieny, J. P. Nozières, Z. Zhang, Y. Liu, and P. P. Freitas, *J. Appl. Phys.* **95**, 6792 (2004).
- ¹⁵J. Ventura, J. Araujo, J. B. Sousa, Y. Liu, Z. Zhang, and P. P. Freitas, *IEEE Trans. Nanotechnol.* (to be published).
- ¹⁶J. Ventura, J. Araujo, J. B. Sousa, Y. Liu, Z. Zhang, and P. P. Freitas, *Appl. Phys. Lett.* (to be published).
- ¹⁷S. Bae, I. F. Tsu, M. Davis, E. S. Murdock, and J. H. Judy, *IEEE Trans. Magn.* **38**, 2655 (2002).
- ¹⁸R. S. Sorbello, in *Solid State Physics*, edited by H. Ehrenreich and F. Spaepen (Springer-Verlag, New York, 1998), Vol. 51, pp.

159–231.

- ¹⁹J. G. Simmons, *J. Appl. Phys.* **34**, 1793 (1963).
- ²⁰E. T. Ogawa, K. D. Lee, V. A. Blaschke, and P. S. Ho, *IEEE Trans. Reliab.* **51**, 403 (2002).
- ²¹C.-L. Liu, X.-Y. Liu, and L. J. Borucki, *Appl. Phys. Lett.* **74**, 34 (1999).
- ²²C. L. Gan, C. V. Thompson, K. L. Pey, W. K. Choi, H. L. Tay, B. Yu, and M. K. Radhakrishnan, *Appl. Phys. Lett.* **79**, 4592 (2001).
- ²³K. S. Ralls, D. C. Ralph, and R. A. Buhrman, *Phys. Rev. B* **40**, 11561 (1989).
- ²⁴O. Céspedes, G. Jan, M. Viret, M. Bari, and J. M. D. Coey, *J. Appl. Phys.* **93**, 8433 (2003).
- ²⁵N. W. Ashcroft and N. D. Mermin, *Solid State Physics*, 5th ed., (New York: Harcourt College Publishing, 1976).
- ²⁶D. N. Bly and P. J. Rous, *Phys. Rev. B* **53**, 13909 (1996).
- ²⁷R. S. Sorbello, *Phys. Rev. B* **39**, 4984 (1989).
- ²⁸H. Kyung, C. S. Yoon, and C. K. Kim, *Mater. Sci. Eng., B* **90**, 13 (2002).
- ²⁹P. LeClair, H. J. M. Swagten, J. T. Kohlhepp, R. J. M. van de Veerdonk, and W. J. M. de Jonge, *Phys. Rev. Lett.* **84**, 2933 (2000).
- ³⁰J. Wang, Y. Liu, P. P. Freitas, E. Snoeck, and J. L. Martins, *J. Appl. Phys.* **93**, 8367 (2003).
- ³¹W. F. Brinkman, R. C. Dynes, and J. M. Rowell, *J. Appl. Phys.* **41**, 1915 (1970).
- ³²B. Chakraborty, W. E. Pickett, and P. B. Allen, *Phys. Rev. B* **14**, 3227 (1976).
- ³³V. Gehanno, P. P. Freitas, A. Veloso, J. Ferreira, B. Almeida, J. B. Sousa, A. Kling, J. C. Soares, and M. F. da Silva, *IEEE Trans. Magn.* **35**, 4361 (1999).
- ³⁴J. Ventura, J. Araujo, J. B. Sousa, Y. Liu, Z. Zhang, and P. P. Freitas (in preparation).
- ³⁵R. C. Sousa, I. L. Prejbeanu, D. Stanescu, B. Rodmacq, O. Redon, B. Dieny, J. Wang, and P. P. Freitas, *J. Appl. Phys.* **95**, 6783 (2004).
- ³⁶R. Ghez, *A Primer of Diffusion Problems* (Wiley, New York, 1988).